ChemComm

COMMUNICATION

View Article Online
View Journal | View Issue

Cite this: *Chem. Commun.*, 2025, **61**, 1617

Received 28th October 2024,
Accepted 20th December 2024

DOI: 10.1039/d4cc05731g

rsc.li/chemcomm

Systematic study of zeolitic imidazolate frameworks for enhanced electrochemical aldehyde sensing†

Martyna Mańka, [ab] Wojciech Kukułka, [c] Mateusz Wlazło, [d] Violetta Patroniak, *[b] Artur Ciesielski, [ac] Verónica Montes-García *[a] and Paolo Samori *[a]

Four distinct zeolitic imidazolate frameworks (ZIFs) are prepared using zinc and cobalt ions with 2-aminobenzimidazole and 2-methylimidazole as linkers to explore their electrochemical properties as platforms for aldehyde detection. The resulting ZIF-based sensors exhibit high sensitivity, low detection limits, and robust performance when applied to real-world samples.

Zeolitic imidazolate frameworks (ZIFs) are a subclass of metal–organic frameworks (MOFs) characterized by the combination of metal ions (commonly zinc or cobalt) and imidazolate-based organic linkers, yielding cage-like three-dimensional structures similar to zeolites.[1] ZIFs combine the high surface area and tunable porosity of MOFs with the thermal and chemical stability of zeolites, endowing them with remarkable versatility.[2] Compared to traditional MOFs, ZIFs offer significantly enhanced stability in water and a wide range of chemical environments, including acidic, basic and solvent-rich conditions. This improved stability not only prolongs their structural integrity but also increases their durability in practical applications, where exposure to harsh or fluctuating conditions is common.[2] As a result, ZIFs are better suited for long-term use in demanding environments, making them more reliable for industrial, environmental, and sensing applications.[3] Among the different sensing technologies, electrochemical sensing offers several advantages: it is typically low-cost, provides rapid and real-time analysis, can be miniaturized for portable applications, and requires relatively simple instrumentation, making it highly suitable for both laboratory and field applications. In electrochemical sensing, ZIFs are especially attractive due to their ultra-high surface areas and tunable pore geometries and sizes.[3] They also offer numerous accessible metal sites and various grafting functional groups capable of interacting with target analytes. Within the various ZIFs, ZIF-8 emerges as a pivotal component.[4] This zinc-based framework composed of zinc nitrate and 2-methylimidazole, has been commonly used as an electrochemical sensor for detecting important small biomolecules,[3] chemical vapors,[5] and metal ions.[4] Despite significant progress, the electrochemical performance of ZIFs remains limited, in particular with respect to sensitivity and selectivity, when compared to conventional analytical methods. This underscores the need for further refinement of ZIF structures and their incorporation into electrochemical systems to improve detection capabilities. The challenge in enhancing the sensitivity and selectivity of ZIFs for sensing applications lies in the need for systematic studies tailored to each target analyte. Achieving the desired performance requires careful tuning of both the metal ion and the organic ligand within the ZIF structure to obtain an effective interaction with specific analytes. However, such comprehensive and systematic studies are currently scarce. Most research tends to focus on general characteristics or broad applications, leaving a significant gap in the detailed optimization required to fully realize the potential of ZIFs in diverse sensing applications. To address this gap, we present a systematic study focusing on the synthesis of four distinct ZIFs, evaluating their physicochemical properties, and optimizing their electrochemical sensing capabilities for the detection of three aldehydes. The importance of this work lies in addressing the pressing need for sensitive and selective detection of aldehydes due to their widespread occurrence and potential health hazards. Specifically formaldehyde,[6] acetaldehyde,[7] and benzaldehyde,[8] are chosen as model analytes in the present case due to their biological significance.[9] Aldehydes in water can be generated during chlorination and ozonation processes, which involve the oxidation of organic matter, or they may leak

[a] *Université de Strasbourg, CNRS, ISIS 8 allée Gaspard Monge, Strasbourg 67000, France. E-mail: montesgarcia@unistra.fr, samori@unistra.fr*
[b] *Faculty of Chemistry, Adam Mickiewicz University, Uniwersytetu Poznańskiego 8, Poznań 61-614, Poland. E-mail: violetta.patroniak@amu.edu.pl*
[c] *Centre for Advanced Technologies, Adam Mickiewicz University, Uniwersytetu Poznańskiego 10, Poznań 61-614, Poland*
[d] *Chemical and Biological Systems Simulation Lab, Centre of New Technologies, University of Warsaw, 02-097 Warsaw, Poland*

† Electronic supplementary information (ESI) available. See DOI: https://doi.org/10.1039/d4cc05731g

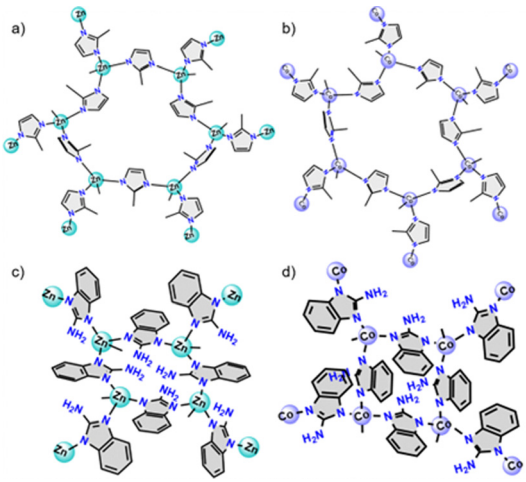

Fig. 1 Schematic structures of (a) ZIF-8, (b) ZIF-67, (c) NH_2-ZIF-7 and (d) NH_2-ZIF-9.

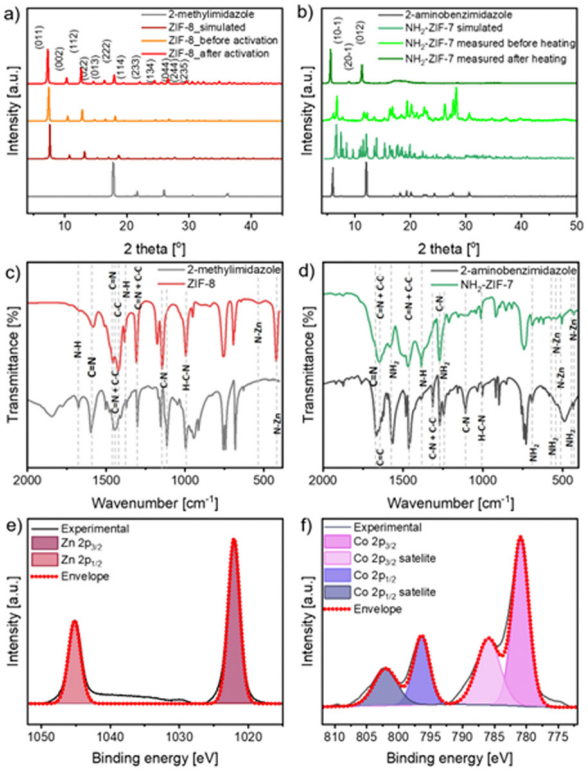

Fig. 2 Normalized PXRD spectra before and after thermal activation of (a) ZIF-8, and (b) NH_2-ZIF-7, normalized FT-IR spectra of (c) ZIF-8 and (d) NH_2-ZIF-7. The simulated PXRD spectra of the ZIFs and the PXRD and FT-IR spectrum of the corresponding organic linker are included for comparison for each ZIF, (e) Zn2p XPS spectrum of ZIF-8 and (f) Co2p XPS spectrum of ZIF-67.

from damaged pipes supplying water to households.[10] Due to their reactivity, aldehydes can form DNA–protein cross-links, potentially leading to carcinogenesis and mutagenesis.[11] According to a 2022 World Health Organization (WHO) report, the tolerable concentration of formaldehyde is set at 2.6 mg L^{-1} in drinking water. Acetaldehyde is classified as a probable human carcinogen by the International Agency for Research on Cancer (IARC). WHO suggest a limit of 0.3 mg m^{-3} (*ca.* 0.25 ppm) for acetaldehyde in indoor environments. Although benzaldehyde is not classified as a carcinogen by major health organizations such as the IARC, prolonged exposure can lead to severe respiratory issues.[8]

Firstly, ZIFs based on 2-methylimidazole and 2-aminobenzimidazole organic linkers with zinc (ZIF-8 and NH_2-ZIF-7 respectively) and cobalt (ZIF-67 and NH_2-ZIF-9 respectively) ions are synthesized by employing reported protocols (Fig. 1 and Fig. S1, ESI†).[12] These four ZIFs will allow us to evaluate the impact of the metal ion and organic linker structure (*i.e.*, both the presence or absence of amino group and benzene ring) on the sensitivity and selectivity toward the detection of three aldehydes. Briefly, a solution containing the metal salt and the organic linker is prepared in methanol and is kept for 24 hours at room temperature under stirring (see ESI† for details). The obtained ZIFs were washed multiple times and finally were thermally activated. The first proof of the successful ZIFs formation is provided by powder X-ray diffraction (PXRD) characterization (Fig. 2a and b and Fig. S2 and S3, ESI†). The XRD patterns of the four ZIFs exhibit high crystallinity and distinct peaks compared to their initial organic building blocks, confirming the successful formation of the ZIF structures. To elucidate the crystal structure of the as-prepared ZIFs and calculate the unit cell parameters (Table S1, ESI†), simulations of the powder XRD patterns using density functional theory (DFT) calculations are performed (Fig. S4, ESI†). The formation of the four ZIFs is then confirmed by Fourier-transform infrared (FTIR) spectroscopy (Fig. 2c and d and Fig. S5–S7, ESI†), where new bands appear at 420 cm^{-1} and 531 cm^{-1} for ZIF-8 and 428 cm^{-1}, 508 cm^{-1} and 538 cm^{-1} for NH_2-ZIF-7, corresponding to the stretching vibrations of N–Zn bond, and bands at 421 cm^{-1} and 533 cm^{-1} for ZIF-67 and 425 cm^{-1}, 502 cm^{-1} and 573 cm^{-1} for NH_2-ZIF-9 corresponding to the stretching vibrations of N–Co bond, which are not present in the organic linkers.[13–15]

To further corroborate the chemical composition of the ZIFs, X-ray photoelectron spectroscopy (XPS) analyses are performed (Fig. 2e and f and Fig. S8–S10, ESI†). The high-resolution N1s spectra of all ZIFs is presented in Fig. S9 (ESI†). On the one hand, ZIF-8 and ZIF-67 show one main peak at 398.9 eV, corresponding to the delocalized C–N–C bond. On the other hand, NH_2-ZIF-7 and NH_2-ZIF-9 display an additional peak at 398 eV, attributed to the primary amines of 2-aminobenzimidazole. Fig. 2e and Fig. S10a (ESI†) show the high-resolution Zn 2p spectra of ZIF-8 (Fig. 2) and NH_2-ZIF-7 (Fig. S10a, ESI†). Both spectra show peaks centered at 1021.76 eV and 1044.71 eV, attributed to Zn $2p_{3/2}$ and Zn $2p_{1/2}$ respectively.[16] Finally, Fig. 2f and Fig. S10b (ESI†) show the high-resolution Co 2p spectra of ZIF-67 (Fig. 2f) and NH_2-ZIF-9 (Fig. S10b, ESI†). The Co 2p spectra can be deconvoluted into two distinct peaks and two weak satellites. The peaks located at 780.88 and 796.98 eV can correspond to Co $2p_{3/2}$ and Co $2p_{1/2}$, respectively. In both cases the space between main and satellite peaks is ~6 eV, which indicates the presence of Co^{2+} in the frameworks.[17] The morphology and microstructure of the as-prepared ZIF materials is evaluated using scanning electron microscopy

(SEM) (Fig. S11, ESI†). The SEM analysis reveals that the ZIFs synthesized from 2-aminobenzimidazole (*i.e.*, NH_2-ZIF-7 and NH_2-ZIF-9) have crystal-like shapes. Differently, the ZIFs synthesized from 2-methylimidazole (*i.e.*, ZIF-8 and ZIF-67) have particle-like shapes, with sizes between 60–110 nm for ZIF-8 and around 500 nm for ZIF-67. Thermogravimetric analysis (TGA) is performed to assess the thermal stability of the samples, as depicted in Fig. S12 (ESI†). A clear difference can be observed for the ZIFs based on 2-methylimidazole and 2-aminobenzimidazole organic linkers. ZIF-8 and ZIF-67 are stable up to temperatures of *ca.* 530 and 500 °C, respectively. Conversely, NH_2-ZIF-7 and NH_2-ZIF-9, begin to decompose at *ca.* 200 °C. The specific surface area (SSA) and pore characteristics of ZIF materials are evaluated through nitrogen adsorption/desorption isotherms, as depicted in Fig. S13 (ESI†). The values of the SSAs and pore sizes can be found in Tables S2 and S3 (ESI†). The isotherms of the four samples exhibit a type IV shape, which is usually attributed to mesoporous materials. However, from the t-plot method values, it is clear that ZIF-8 and ZIF-67 are composed of a significant majority of micropores (>93%). Furthermore, while the isotherms of ZIF-8 and NH_2-ZIF-9 exhibit an H3 type hysteresis loop, indicating the presence of loosely assembled particles forming slit-like pores, ZIF-67 and NH_2-ZIF-7 exhibit an H4 type hysteresis loop, which, likewise H3, also indicates the presence of slit-like pores but with a higher contribution of micropores, as confirmed in the *t*-plot method values.[18] Interestingly the two ZIFs based on 2-methylimidazole organic linker, ZIF-8 and ZIF-67, display the highest SSA (*ca.* 1575 $m^2\ g^{-1}$ in both cases), together with the largest total pore volume, 0.84 and 0.59 $cm^3\ g^{-1}$, respectively. Finally, through the Horvath–Kawazoe method, the average micropore diameter for ZIF-8 and ZIF-67 is calculated to be 1.23 and 1.20 nm, respectively. Before conducting electrochemical sensing of specific aldehydes, the chemical stability and aldehyde's sensing mechanism of the four ZIFs are assessed. Powder ZIFs are dispersed in aldehyde solutions and stirred for 24 hours (see ESI,† for details).[19] Subsequently, the ZIFs are washed, and their chemical stability is evaluated using XRD (Fig. S14 and S15, ESI†) and XPS analyses (Fig. S16–S19, ESI†). As can be seen in Fig. S15 (ESI†), all the ZIFs demonstrate stability in the different aldehyde solutions, as their PXRD diffractograms remain unchanged. XPS analysis clearly confirms the formation of an imine bond between the amino group of ZIF and the carbonyl group of the aldehyde in the case of NH_2-ZIF-7 and NH_2-ZIF-9. This is shown by a decrease in the intensity of the C–NH_2 band at 398 eV with a simultaneous increase in the intensity of the C–N–C band at 398.9 eV. The small pore volumes of NH_2-ZIF-7 and NH_2-ZIF-9 prevent the entrapment of aldehyde molecules within their structure. However, the presence of the C=O peak at 287.5 eV in their high-resolution C1s spectra (Fig. S18 and S19, ESI†) suggests that, in addition to imine bond formation, aldehyde molecules are adsorbed on the surface. In contrast, for ZIF-8 and ZIF-67, aldehydes can be captured within their structure due to their larger pore sizes. This is evidenced by the presence of a much weaker C=O signal compared to the one obtained for NH_2-ZIF-7 and NH_2-ZIF-9. This indicates a lower presence of aldehydes in the ZIFs surface. Importantly, as XPS is a surface technique (penetration depth of 3–10 nm), the signals from aldehydes that are trapped inside the ZIFs cannot be detected. The electrochemical sensing performance of ZIFs toward specific aldehydes is assessed in a three-electrode system where ZIFs act as the working electrode, Pt as the counter electrode and Ag/AgCl as the reference electrode. These electrodes are immersed in a mixture of electrolyte (*i.e.*, potassium hexacyanoferrate(III)) and a certain aldehyde concentration (0–1 mM) (see ESI† for details). After five minutes of incubation, electrochemical impedance spectroscopy (EIS) is measured and the performance is expressed as capacitance (C_p) (see eqn (S1), ESI†). Although the electrochemical performance of MOF-based sensors is typically reported using ionic conductivity,[20] we select capacitance as the primary measurement parameter because it allows for straightforward, direct interpretation without requiring complex fitting or modeling. The electrochemical sensing performance of the different ZIFs can be seen in: ZIF-8 (Fig. 3a–c and Fig. S20, ESI†), ZIF-67 (Fig. S21, ESI†), NH_2-ZIF-7 (Fig. S22, ESI†) and NH_2-ZIF-9 (Fig. S23, ESI†). The C_p-frequency response of all ZIFs indicates that 0.1 Hz is the optimal frequency, displaying the greatest C_p increase with increasing aldehyde concentration. Therefore, in order to calculate the sensitivity of each ZIF, the normalized capacitance at 0.1 Hz is plotted as a function of the specific aldehyde concentration. As shown in Fig. 3b and Fig. S20–S23 (ESI†), in almost all cases, a saturation level is reached, meaning the capacitance no longer increases with aldehyde concentration, at concentrations above *ca.* 100 μM. The key performance indicators of the electrochemical sensing performance of ZIFs can be found in Tables S4–S7 (ESI†) and Fig. 3d. As shown in Fig. 3d, ZIFs synthesized from 2-aminobenzimidazole (*i.e.*, NH_2-ZIF-7 and NH_2-ZIF-9) exhibit higher sensitivity toward the three aldehydes compared to those synthesized from 2-methylimidazole (*i.e.*, ZIF-8 and ZIF-67). In some cases, the sensitivity difference is modest (*e.g.*, between ZIF-8 and NH_2-ZIF-7 towards formaldehyde, or ZIF-67 and NH_2-ZIF-9 towards acetaldehyde), but in others, the increase is

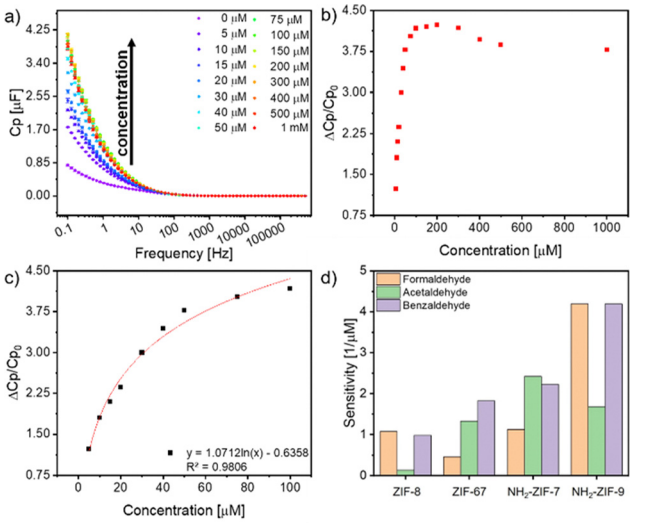

Fig. 3 (a) Capacitance response, (b) normalized capacitance response ($\Delta C_p/C_{p_0}$) and (c) logarithmic fitting in the calibration range of 5–100 μM of ZIF-8 as a function of the concentration of formaldehyde, (d) sensitivity of ZIF-based sensors to selected aldehydes.

substantial—ranging from 2 to 5 times (*e.g.*, ZIF-8 *vs.* NH_2-ZIF-7 for acetaldehyde, or ZIF-67 *vs.* NH_2-ZIF-9 for benzaldehyde). Although ZIF-8 and ZIF-67 possess higher surface area and porosity, their performance in aldehyde detection is inferior to that of NH_2-ZIF-7 and NH_2-ZIF-9. In ZIF-8 and ZIF-67, aldehydes primarily interact *via* hydrogen bonding, while in NH_2-ZIF-7 and NH_2-ZIF-9, aldehydes engage not only by hydrogen bonding but also by imine bond formation and π–π interactions in the case of benzaldehyde, leading to enhanced detection performance. For Co-based ZIFs, a notable trend is observed where sensitivity increases with the size of the aldehyde molecule, with formaldehyde showing the lowest sensitivity and benzaldehyde the highest. In contrast, Zn-based ZIFs do not exhibit a similar consistent trend in sensitivity. From these findings, it can be concluded that NH_2-ZIF-7 demonstrates the highest sensitivity toward smaller aldehydes such as formaldehyde and acetaldehyde, while NH_2-ZIF-9 excels in detecting larger aldehydes, particularly benzaldehyde. Additionally, limits of detection in the micromolar range are achieved for the three aldehydes (Tables S4–S7, ESI†), highlighting the ZIFs' effectiveness in low-concentration detection. Finally, the robustness of ZIF-based electrochemical sensors is evaluated using a real-world sample, specifically tap water. Different concentrations of aldehydes are spiked into filtered tap water, and the capacitance is measured. The aldehyde concentrations are then determined using the previously established logarithmic regressions. In agreement with the previous analysis in Milli Q water, the best results are obtained for NH_2-ZIF-7 and NH_2-ZIF-9. As shown in Table S8 (ESI†), the recovery rates for aldehydes are consistently above 90%, demonstrating the robustness of ZIF-based electrochemical sensors.[21]

In summary, we have revealed that NH_2-ZIF-7 and NH_2-ZIF-9 show significantly higher sensitivity to aldehydes than ZIF-8 and ZIF-67, despite the latter having larger surface areas ($\sim$1500 $m^2\ g^{-1}$ *vs.* $<$ 30 $m^2\ g^{-1}$ of NH_2-ZIF-7 and NH_2-ZIF-9). The enhanced performance of NH_2-based ZIFs is attributed to both hydrogen bonding and imine bond formation with aldehydes. Furthermore, these electrochemical sensors demonstrated limits of detection in the micromolar range and robust performance in real sample analyses without the need for complex sample preparation, which is typically required in chromatographic methods. This work paves the way for future sensor optimization to achieve the highest sensitivity in electrochemical sensors based on ZIFs, enabling their application to a broader range of environmental and biologically-relevant analytes.

This work was supported by French government scholarship France Excellence, by the National Science Centre (grant no. 2022/47/B/ST4/02310), by Agence Nationale de la Recherche through the Interdisciplinary Thematic Institute SysChem *via* the IdEx Unistra (ANR-10-IDEX-0002) within the program Investissement d'Avenir and the Foundation Jean-Marie Lehn. We also gratefully acknowledge Poland's high-performance computing infrastructure PLGrid (HPC Centers: ACK Cyfronet AGH) for providing computer facilities and support within computational grant no. PLG/2022/015965, and PLGrid for awarding this project access to the LUMI super-computer, owned by the EuroHPC Joint Undertaking, hosted by CSC (Finland) and the LUMI consortium through grant no. PLL/2022/03/016435.

Data availability

Data available on request from the authors. The data that support the findings of this study are available from the corresponding author, Paolo Samorì, upon reasonable request.

Conflicts of interest

There are no conflicts to declare.

Notes and references

1 J. Yao and H. Wang, *Chem. Soc. Rev.*, 2014, **43**, 4470–4493.
2 Y. V. Kaneti, S. Dutta, M. S. A. Hossain, M. J. A. Shiddiky, K.-L. Tung, F.-K. Shieh, C.-K. Tsung, K. C.-W. Wu and Y. Yamauchi, *Adv. Mater.*, 2017, **29**, 1700213.
3 Z. Feng, H. N. Lim, I. Ibrahim and N. S. K. Gowthaman, *J. Mater. Chem. B*, 2023, **11**, 9099–9127.
4 A. Paul, I. K. Banga, S. Muthukumar and S. Prasad, *ACS Omega*, 2022, **7**, 26993–27003.
5 G. Lu and J. T. Hupp, *J. Am. Chem. Soc.*, 2010, **132**, 7832–7833.
6 S. T. S. Arsawiset, *Anal. Chim. Acta*, 2020, **1118**, 63–72.
7 A. T. Cartus, D. W. Lachenmeier, S. Guth, A. Roth, M. Baum, P. Diel, G. Eisenbrand, B. Engeli, M. Hellwig, H.-U. Humpf, H.-G. Joost, S. E. Kulling, A. Lampen, D. Marko, P. Steinberg, W. Wätjen, J. G. Hengstler and A. Mally, *Mol. Nutr. Food Res.*, 2023, **67**, 2200661.
8 C. O. Phillips, Y. Syed, N. M. Parthaláin, R. Zwiggelaar, T. C. Claypole and K. E. Lewis, *J. Breath Res.*, 2012, **6**, 036003.
9 Y. K. Jo, S.-Y. Jeong, Y. K. Moon, Y.-M. Jo, J.-W. Yoon and J.-H. Lee, *Nat. Commun.*, 2021, **12**, 4955.
10 *Guidelines For Drinking Water Quality*, World Health Organization, Geneva.
11 Y. Oka, Y. Nakazawa, M. Shimada and T. Ogi, *Nat. Cell Biol.*, 2024, **26**, 784–796.
12 A. Deacon, L. Briquet, M. Malankowska, F. Massingberd-Mundy, S. Rudić, T. L. Hyde, H. Cavaye, J. Coronas, S. Poulston and T. Johnson, *Commun. Chem.*, 2022, **5**, 18.
13 C. Valentini, V. Montes-García, L. Cusin, D. Pakulski, M. Wlazło, P. Samorì and A. Ciesielski, *Small Sci.*, 2024, **4**, 2400031.
14 D. Pakulski, V. Montes-García, A. Gorczyński, W. Czepa, T. Chudziak, M. Bielejewski, A. Musiał, I. Pérez-Juste, P. Samorì and A. Ciesielski, *J. Mater. Chem. A*, 2024, **12**, 440–450.
15 F. B. Jayashree Ethiraj, C. Lamberti and S. Bordiga, *Microporous Mesoporous Mater.*, 2015, **207**, 90–94.
16 S. Deng, G. Yu, S. Xie, Q. Yu, J. Huang, Y. Kuwaki and M. Iseki, *Langmuir*, 2008, **24**, 10961–10967.
17 R. Chen, S. Luo, Y. Xia and L. Xiang, *J. Environ. Chem. Eng.*, 2024, **12**, 112497.
18 K. S. W. Sing, *Pure Appl. Chem.*, 1985, **57**, 603–619.
19 G. L.-C. K. Caamaño, R. Heras-Mozos, J. Glatz, P. Hernández-Muñoz, R. Gavara and M. Giménez-Marqués, *Dalton Trans.*, 2023, **52**, 17993–17999.
20 J. J. Gassensmith, J. Y. Kim, J. M. Holcroft, O. K. Farha, J. F. Stoddart, J. T. Hupp and N. C. Jeong, *J. Am. Chem. Soc.*, 2014, **136**, 8277–8282.
21 Z.-Y. Han, H. Zhang, H.-K. Li, Q.-Q. Zhu and H. He, *J. Mater. Chem. C*, 2021, **9**, 4576–4582.

